Drug Delivery

ISSN: (Print) (Online) Journal homepage: informahealthcare.com/journals/idrd20

Photo-crosslinkable polyester microneedles as sustained drug release systems toward hypertrophic scar treatment

Anna Szabó, Ignace De Decker, Sam Semey, Karel E.Y. Claes, Phillip Blondeel, Stan Monstrey, Jo Van Dorpe & Sandra Van Vlierberghe

To cite this article: Anna Szabó, Ignace De Decker, Sam Semey, Karel E.Y. Claes, Phillip Blondeel, Stan Monstrey, Jo Van Dorpe & Sandra Van Vlierberghe (2024) Photo-crosslinkable polyester microneedles as sustained drug release systems toward hypertrophic scar treatment, Drug Delivery, 31:1, 2305818, DOI: 10.1080/10717544.2024.2305818

To link to this article: https://doi.org/10.1080/10717544.2024.2305818

DRUG DELIVERY
2024, VOL. 31, NO. 1, 2305818
https://doi.org/10.1080/10717544.2024.2305818

Taylor & Francis
Taylor & Francis Group

RESEARCH ARTICLE

OPEN ACCESS Check for updates

Photo-crosslinkable polyester microneedles as sustained drug release systems toward hypertrophic scar treatment

Anna Szabó[a], Ignace De Decker[b,c], Sam Semey[a], Karel E.Y. Claes[b,c], Phillip Blondeel[b,c], Stan Monstrey[b,c], Jo Van Dorpe[d] and Sandra Van Vlierberghe[a]

[a]Polymer Chemistry and Biomaterials Group, Centre of Macromolecular Chemistry (CMaC), Department of Organic and Macromolecular Chemistry, Ghent University, Ghent, Belgium; [b]Burn Center, Ghent University Hospital, Ghent, Belgium; [c]Department of Plastic Surgery, Ghent University Hospital, Ghent, Belgium; [d]Department of Pathology, Ghent University Hospital, Ghent, Belgium

ABSTRACT

Burn injuries can result in a significant inflammatory response, often leading to hypertrophic scarring (HTS). Local drug therapies e.g. corticoid injections are advised to treat HTS, although they are invasive, operator-dependent, extremely painful and do not permit extended drug release. Polymer-based microneedle (MN) arrays can offer a viable alternative to standard care, while allowing for direct, painless dermal drug delivery with tailorable drug release profile. In the current study, we synthesized photo-crosslinkable, acrylate-endcapped urethane-based poly(ε-caprolactone) (AUP-PCL) toward the fabrication of MNs. Physico-chemical characterization (^{1}H-NMR, evaluation of swelling, gel fraction) of the developed polymer was performed and confirmed successful acrylation of PCL-diol. Subsequently, AUP-PCL, and commercially available PCL-based microneedle arrays were fabricated for comparative evaluation of the constructs. Hydrocortisone was chosen as model drug. To enhance the drug release efficiency of the MNs, Brij®35, a nonionic surfactant was exploited. The thermal properties of the MNs were evaluated via differential scanning calorimetry. Compression testing of the arrays confirmed that the MNs stay intact upon applying a load of 7 N, which correlates to the standard dermal insertion force of MNs. The drug release profile of the arrays was evaluated, suggesting that the developed PCL arrays can offer efficient drug delivery for up to two days, while the AUP-PCL arrays can provide a release up to three weeks. Finally, the insertion of MN arrays into skin samples was performed, followed by histological analysis demonstrating the AUP-PCL MNs outperforming the PCL arrays upon providing pyramidical-shaped perforations through the epidermal layer of the skin.

GRAPHICAL ABSTRACT

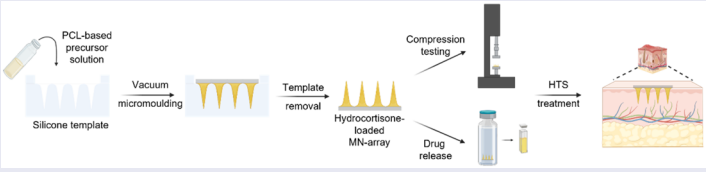

HIGHLIGHTS

- AUP-PCL MN arrays provide long-term transdermal drug delivery of hydrocortisone
- AUP-PCL-based MN arrays provide superior drug release profiles compared to PCL MNs
- Effective skin penetration AUP-PCL-based MNs on skin was achieved

ARTICLE HISTORY
Received 27 July 2023
Revised 10 October 2023
Accepted 22 December 2023

KEYWORDS
Microneedles; polyester; cortisone; hypertrophic scarring; controlled drug release; intradermal drug delivery

1. Introduction

Hypertrophic scarring (HTS) is a common sequela after burns. Due to severe physical limitations and cosmetic disfigurements, HTS frequently impedes the patients' rehabilitation and reintegration into society (De Decker et al., 2023a, 2023b, 2023d). Both prophylactic and curative scar management therapies are available. Conservative scar management has a trifold approach: protection from ultraviolet radiation, hydration and pressure therapy using garments with or without inlays or additional paddings. When this does not suffice, there can be opted for (minimally) invasive treatments. Intracicatrical drug therapy is still considered the most effective compared to other more invasive treatments. Ever since

CONTACT Sandra Van Vlierberghe Sandra.VanVlierberghe@ugent.be Polymer Chemistry and Biomaterials Group, Centre of Macromolecular Chemistry (CMaC), Department of Organic and Macromolecular Chemistry, Ghent University, Ghent, Belgium
Supplemental data for this article can be accessed online at https://doi.org/10.1080/10717544.2024.2305818.

the 1960s, the intracicatrical administration of corticoids by injection, has been the 'go-to' when conservative management fails (De Decker et al., 2023d; Gauglitz et al., 2011). However, injections are extremely painful, operator-dependent and do not have a uniform drug distribution pattern, which can cause undesired side effects including atrophy, angiotelectasis and calcification (De Decker et al., 2023d; Gauglitz et al., 2011; Lin et al., 2019).

Microneedle (MN) arrays are minimally invasive medical devices with micron-scaled needle-like projections in a size range of 150 to 1000 µm in length. They offer direct drug delivery to the dermis, therefore, enhancing transdermal delivery efficiency of therapeutical drugs, while preventing the stimulation of pain receptors (Tan et al., n.d; Lin et al., 2019; Du and Sun, 2020; Bhadale and Londhe, 2021). To date, several MN alternatives are available, namely solid, dissolvable, hollow, coated and hydrogel microneedles (Nagarkar et al., 2020; Aldawood et al., 2021; De Decker et al., 2023c; Koyani, 2020; Prausnitz, 2004). They provide various drug delivery mechanisms and efficiencies in line with their applications. The first type of microneedle arrays was the group of solid microneedles, which are typically fabricated of biocompatible metals or silicone. Solid MN arrays can efficiently penetrate the stratum corneum, while inflicting microchannels in the upper dermis to increase the permeability of the dermis toward pharmaceuticals (Nagarkar et al., 2020; Prausnitz, 2004).

Over the past decade, polymer-based solid microneedle arrays advanced. Biocompatible, biodegradable non-hydrophilic polymers, like poly(lactic acid) (PLA), poly(glycolic acid) (PGA) and poly(lactide-co-glycolic acid) (PLGA) have drawn attention thanks to their sufficient skin penetration strength and mass processability (Koyani, 2020). Moreover, PLA MN arrays have showed efficient transdermal insulin delivery, while PGA MNs have already been exploited for transdermal vaccination. PLGA-based MN arrays were proven to support long-term controlled drug release of hydrophobic pharmaceuticals (Park et al., 2006), although their application in the state-of-the-art remains limited (Koyani, 2020), as poly(ε-caprolactone)-based (PCL) MN arrays can offer similar properties combining thermostability, and low melting point, resulting in more efficient processability; moreover, its utilization is cost-efficient. Poly(ε-caprolactone)-based MN arrays (Andersen et al., 2018) were proven to provide sufficient transdermal delivery toward cosmetic applications (Ko et al., n.d), skin cancer treatment (Cheng et al., 2017) and pH responsive gene delivery (Li et al., 2019). Ko et al. developed PCL (Mn = 70–90 kg/mol, Mw = 80 kg/mol) and PCL/poly(ethylene glycol) (PEG) blend-based MN arrays to encapsulate hydrophilic drugs, rhodamine-6G and FITC-collagen. The PCL 80 kg/mol-based MN arrays were able to withstand the skin insertion force applied on the arrays and provided continuous drug release of the encapsulated compounds up to 96 hours (Ko et al., n.d). However, to date, hypertrophic scarring was not involved in the applications of PCL-based MN arrays.

To further improve the skin penetration efficacy of PCL, photo-crosslinkable PCL-based polymers can offer a viable alternative. The introduction of chemical crosslinking points thereby forming a polymer network significantly increases the stiffness of the material, whilst maintaining its biocompatibility (Arslan et al., 2021). Thijssen et al. reported a PCL-based (Mn = 2000 g/mol) acrylate-endcapped urethane-based polymer with a Young's modulus of 38.7 ± 4.1 MPa (Thijssen et al., 2022), which corresponds to an approximate 5-fold modulus increase compared to unmodified PCL Mn = 2000 g/mol (6.3 ± 0.3 MPa; Arslan et al., 2021) upon crosslinking of two acrylate end group functionalities on each PCL chain. Upon introducing multifunctional end-capping agents (ethoxylated and propoxylated pentaerythritol triacrylate, EPPETA, 6 acrylates per chain) on PCL, the Young's modulus further increases up to 57.8 ± 2.9 MPa, which implies, that the stiffness can be fine-tuned through the crosslink density (Arslan et al., 2021). Moreover, AUP materials have shown solid-state photo-crosslinkability in the presence of photoinitiators (Arslan et al., 2021; Houben et al., 2014), allowing for the fabrication of low molar mass AUP-PCLs (M_n = 530 g/mol) toward microneedle fabrication exploiting solvent-free conditions, while offering shape fidelity to the structures.

Thus far, hypertrophic burn wound treatment involved the application of electrospun PCL-based wound dressings (Lorden et al., 2015), in combination with gelatin for the delivery of TGF-β-1 inhibitor (Wang et al., 2017) or palmitine (Jiang et al., 2021). Another attempt was reported by Lin et al., which involved the application of 5-fluorouracil- and triamcinolone-loaded hydroxypropyl-β-cyclodextrin enriched hyaluronic acid (HA) microneedles to heal HTS, modeled on rabbit ear *ex vivo* (Lin et al., 2019). De Decker et al. reported the first clinical pilot study of corticosteroid-loaded hyaluronic acid-based dissolving microneedle arrays. They successfully maintained a faster and improved healing profile on HTS during 4 months of therapy, involving 4 MN-insertion treatments. The applied HA-based MN arrays were correlating with a drug load of 0.89 mg/cm^2, and the active compound was intradermally delivered within 30 minutes following insertion of the arrays (De Decker et al., 2023c).

The current study aims to develop a solid, PCL-based MN array for corticosteroid-based intradermal HTS treatment toward a long-term drug release profile up to 21 days. To this end, a commercially available, FDA-approved PCL with an average molar mass of 80 kg/mol was exploited for MN fabrication and was compared with an in-house developed, multifunctional PCL-based acrylate-endcapped urethane-based polymer (AUP-PCL) with a PCL backbone having a molar mass of 530 g/mol. The aim was to enable comparison of the two PCL-based polymers for their potential toward microneedle fabrication, mechanical strength, and extended drug release. Hydrocortisone was applied in the microneedle arrays as model drug to treat hypertrophic scarring. Drug release of the active compound was investigated for 3 weeks exploiting different drug loadings (varying between 1 and 3 mg/MN array). Moreover, Brij®35 was exploited as additive, since non-ionic surfactants can improve the drug release profile with regards to efficacy and elongation from MN arrays (Yavuz et al., 2020). Finally, the penetration of the developed MN arrays on *ex vivo* skin samples was evaluated, followed by histological evaluation.

2. Materials and methods

1.1. Materials

Poly(ε-caprolactone) (PCL, Mn = 80 kg/mol), poly(ε-caprolactone) diol (Mn = 530 g/mol), isophorone diisocyanate (IPDI), triphenylphosphine (TPP), phenothiazine (PTZ), dimethylterephthalate (DMT), Brij®35 and phosphate buffered saline (PBS) were purchased from Merck (Belgium). 2,6-di-tert-butyl-4-methylphenol (BHT) was obtained from Innochem (Belux). Deuterated chloroform was purchased from EurIsotop (Belgium). Ethoxylated and propoxylated pentaerythritol triacrylate (EPPETA) and bismuth neodecanoate catalyst were kindly provided by Allnex (Belgium). Diphenyl(2,4,6-trimethylbenzoyl)phosphine oxide (TPO-L) was provided by Lambson (UK). Chloroform and acetone were purchased from ChemLab (Belgium). Hydrocortisone was purchased from the Apothecary of the Ghent University Hospital, (UZ Ghent, Ghent, Belgium). The skin samples were obtained from residual waste from a subcutaneous mastectomy. Small containers with 10% formol were purchased from VWR Chemicals (Fontenay-Sous-Bois, France) and automatic hematoxylin and eosin (HE) staining of the paraffin slices was used (T181 Tissue- Tek Prisma Plus, Sakura Finetek, Antwerp, Belgium).

1.2. Synthesis of acrylate-endcapped urethane-based poly(ε-caprolactone)

AUP-PCL (Figure 2) was developed based on a previously reported protocol from our group (Vermoesen et al., 2023). In brief, one-pot synthesis was performed in bulk. PCL diol with a molar mass of 530 g/mol was chosen as polymer backbone. 0.4 mol PCL diol (200 g) was reacted with two molar equivalents (0.8 mol, 168 g) of IPDI at 75 °C under inert atmosphere for 2 hours, in the presence of bismuth neo-decanoate as catalyst (600 ppm) to introduce urethane groups on the -OH functionalities of the backbone. Next, two molar equivalents of EPPETA functioning as endcapping agent (0.8 mol, 432 g) were added dropwise under vigorous stirring, in the presence of bismuth neodecanoate catalyst (additional 600 ppm) to form another urethane functionality with the free -NCO moiety of the IPDI units. Subsequently, TPP and PTZ were added as post-stabilizers (1000 ppm each). The nomenclature of the product will be AUP-PCL530-HA throughout the manuscript.

1.3. Physico-chemical characterization of AUP-PCL

1.3.1. Structural analysis and molar mass determination via proton nuclear magnetic resonance (^{1}H-NMR) spectroscopy

The chemical structure of the AUP-PCL530-HA was determined via ^{1}H-NMR spectroscopy (Bruker Avance 300 MHz Spectrometer) in the presence of DMT as internal standard (10 mg/ml concentration for both components) in deuterated chloroform as solvent. The characteristic peaks in the spectrum were allocated to the different parts of the molecular structure (Figure 2). The spectrum was analyzed with the help of MestReNova software. The acrylate content ($M_{acry.}$, mmol acrylate/g AUP) was determined based on the integrals of the characteristic DMT and acrylate peaks and using the following equation (Eq. (1)):

$$M_{acry.} = \frac{I_{\delta=5.83ppm} + I_{\delta=6.12ppm} + I_{\delta=6.40ppm}}{I_{\delta=8ppm}} \cdot \frac{N_{H,\delta=8ppm}}{N_{\delta=5.83ppm} + N_{\delta=6.12ppm} + N_{\delta=6.40ppm}} \cdot \frac{W_{DMT}}{MW_{DMT}} \cdot \frac{1000}{W_{AUP}} \quad (1)$$

where I_δ = 5.83 ppm + I_δ = 6.12 ppm + I_δ = 6.40 ppm refers to the sum of the signal integrals of the protons present in the

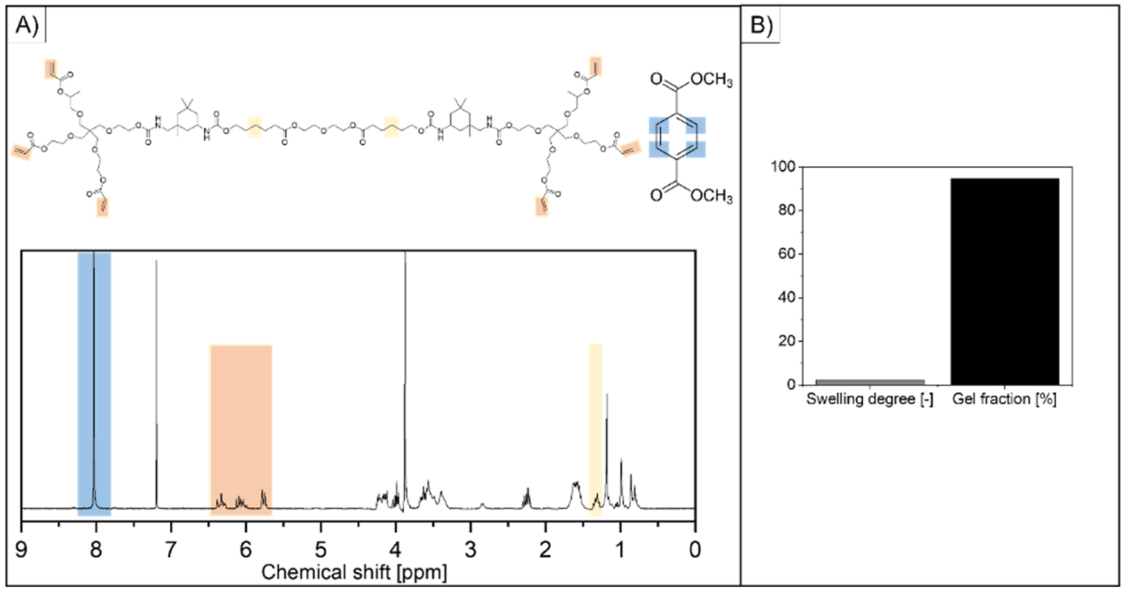

Figure 2. Physico-chemical characterization of the developed AUP-PCL530-HA polymer. (A) shows the ^{1}H-NMR spectrum of the product (the representative peaks are highlighted in yellow for the PCL backbone and in orange for the acrylate moieties) and of dimethyl terephthalate (DMT, internal standard, the representative peak is highlighted in blue). The acrylate content (2.17 mmol/g AUP-PCL530-HA) and molar mass (Mw = 2600 g/mol) of the product were evaluated based on the highlighted integrals and of Eqs. (1)–(2) and are in line with previous reports (O'Neil, 2001). (B) represents the swelling degree and gel fraction of the final product. The swelling degree implied limited swelling in chloroform, while the gel fraction suggested efficient photo-crosslinking.

acrylates (δ = 5.83, 6.12 and 6.40 ppm), I_δ = 8 ppm refers to the signal integral of the protons from the aromatic ring in DMT (δ = 8 ppm), N_δ = 5.83 ppm + N_δ = 6.12 ppm + N_δ = 6.40 ppm equals the number of protons present in the acrylate end groups, N_H, δ = 8 ppm is the number of protons in the benzene ring of DMT, W_{DMT} is the mass of DMT (g), W_{AUP} is the mass of AUP (g) and MW_{DMT} is the molar mass of DMT (194.186 g/mol).

Subsequently, the molar mass of the AUP-PCL530-HA product was determined using Eq. (2):

$$M_w\left(\frac{g}{mol}\right)=\left[\left(\frac{I_{\delta=1.40ppm}}{I_{\delta=5.83ppm}+I_{\delta=6.12ppm}+I_{\delta=6.40ppm}}\right)\cdot\left(\frac{N_{\delta=5.83ppm}+N_{\delta=6.12ppm}+N_{\delta=6.40ppm}}{N_{\delta=1.40ppm}}\right)\cdot W_{PCL^-diol}\right]+103.43+\left(W_{IPDI}\cdot(X+1)+(2\cdot W_{EPPETA})\right) \quad (2)$$

where I_δ = 5.83 ppm + I_δ = 6.12 ppm + I_δ = 6.40 ppm refers to the sum of the signal integrals of the protons present in the acrylates (δ = 5.83, 6.12 and 6.40 ppm), I_δ = 1.40 ppm refers to the signal integral of the protons from the methylene group in the ε-caprolactone units (δ = 1.40 ppm), N_δ = 5.83 ppm + N_δ = 6.12 ppm + N_δ = 6.40 ppm equals the number of protons present in the acrylate end groups, $N_{H,\ \delta=1.40ppm}$ is the number of protons in the methylene group in the ε-caprolactone units (δ = 1.40 ppm), $W_{monomer}$ is the molar mass of the PCL-diol unit (in g/mol), W_{IPDI} and W_{EPPETA} are the molar mass of isophorone diisocyanate and the acrylate endcap, respectively (in g/mol). The endcap was built in on both sides of the PCL diol backbone. Therefore, the W_{EPPETA} was multiplied by 2. X depicts the repeating backbone unit of the PCL-diol-IPDI units, and 103.43 g. mol^{-1} is the molar mass of the PCL-diol initiator molecule.

1.3.2. Swelling and gel fraction experiments

To determine the swelling capacity and gel fraction of the photo-crosslinked AUP-PCL530-HA in the presence of chloroform as solvent, first 1 mm-thick sheets of AUP-PCL-HA were film-casted. In brief, 1 g AUP-PCL530-HA was dissolved in 5 ml chloroform and supplemented with TPO-L as photoinitiator in a 2 mol% concentration with respect to the double bonds present in the material (2.17 mmol/g). Chloroform was evaporated from the sample and afterwards, the AUP-PCL530-HA was transferred between 2 parallel glass plates covered with Teflon foil, separated with a 1 mm silicone spacer. AUP-PCL530-HA was UV-A irradiated for 30 min (λ = 365 nm, I = 7.5 mW/cm^2). Subsequently, disks of 7 mm diameter were punched out and dried under vacuum. Dry AUP-PCL530-HA disks were weighed (w_{d1}) and afterwards incubated in chloroform for 24 hours. The mass of the swollen samples was determined (w_s) and finally, the swollen samples were vacuum dried and weighed (w_{d2}). The swelling degree and gel fraction were determined with the following equations (Eq. (3)–(4)):

$$Swelling\ degree[-]=\frac{w}{w_{d2}} \quad (3)$$

$$Gel\ fraction[\%]=\frac{w_{d,2}}{w_{d,1}}\cdot 100\% \quad (4)$$

1.4. Fabrication and characterization of PCL-based MN arrays

For the development and fabrication of the MN arrays, two starting materials were applied, including AUP-PCL530-HA and PCL 80 kg/mol. In the following section, the fabrication and characterization of the two types of MN arrays will be described.

To characterize the drug release profile from the microneedle arrays, a corticosteroid i.e., hydrocortisone (HC), was chosen as model drug. In order to further tune the drug release profile of the hydrocortisone, Brij®35, a nonionic surfactant was applied as solubility enhancer (Yavuz et al., 2020). Table 1 summarizes the developed PCL-based MN precursor formulations with respect to their drug and solubility enhancer content, as well as to the applied solvents. The listed solutions were exploited for MN array fabrication throughout the manuscript.

1.4.1. Preparation of MN array precursor solutions

500 mg AUP-PCL530-HA or PCL 80 kg/mol was incorporated in the formulations indicated in Table 1. When preparing AUP-PCL530-HA solutions, TPO-L as photoinitiator was also added in 2 mol% concentration with respect to the double bonds present in the material (2.17 mmol/g). The amount of solvent applied was calculated based on the solubility of HC (O'Neil, 2001) (1.6 mg/ml in chloroform and 9.3 mg/ml in acetone).

1.4.2. Vacuum molding of PCL-based compositions

PDMS molds, kindly provided by Smicna Pte. Ltd (Singapore), were exploited with an array surface area of 10 × 10 mm^2, 6 on 6 MN array, with MN cavities of 1000 µm height and 500 µm pillar base width with 300 µm interpillar distance. In order to fabricate solid microneedle arrays with an active compound cargo only in the needles, fractional molding was performed in a BINDER Vacuum drying chamber (Figure 1). Prior to molding, different solutions of PCL-based samples were prepared (as indicated in Table 1).

In case of the PCL 80 kg/mol-based samples, a 30 wt% solution was applied for molding (note that the samples were dissolved in a larger amount of chloroform 3–15 wt%, see Table 1; therefore, the excess solvent was evaporated from the samples) to fill the needle cavities. Subsequently, the solutions were transferred onto the molds and placed in the vacuum oven at 60 °C. In order to achieve efficient penetration of the PCL 80 kg/mol into the microneedle cavities, the above-mentioned step was repeated 2 times. Afterwards, the excess of the molding solution was removed from the molds, and the base of the microneedle arrays was filled with blank PCL 80 kg/mol solutions (30 wt%). The samples were air-dried overnight and removed from the molds the following day.

Table 1. List of the developed PCL-based MN precursor formulations utilized during molding.

PCL type	Hydrocortisone (HC) content (mg/mg polymer)	Hydrocortisone (HC) content (mmol/mmol polymer)	**Brij®35 content (µl/mg polymer)**	**Brij®35 content (mmol/mmol polymer_**	Solvent	Amount of solvent (ml)
PCL 80 kg/mol	–	–	–	–	Chloroform	5
	50/500	0.14/0.01	–	–		25
	–	–	50/500	0.04/0.01		5
	50/500	0.14/0.01	50/500	0.04/0.01		25
AUP-PCL530-HA	–	–	–	–	Acetone	5
	50/500	0.14/0.19	–	–		6
	–	–	50/500	0.04/0.19		5
	50/500	0.14/0.19	50/500	0.04/0.19		6
	125/500	0.34/0.19	–	–		14
	125/500	0.34/0.19	50/500	0.04/0.19		14
	250/500	0.69/0.19	–	–		28
	250/500	0.69/0.19	50/500	0.04/0.19		28

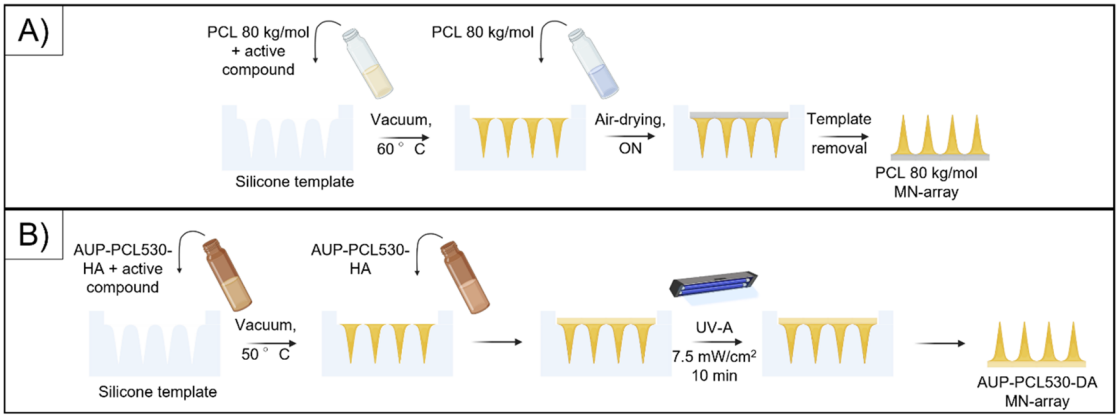

Figure 1. Scheme representing the molding procedure. (a) represents the vacuum molding of the PCL 80 kg/mol-based MN arrays, while (b) shows the vacuum molding procedure for the AUP-PCL530-HA-based MN arrays. The illustration was prepared with Biorender.

In case of the AUP-PCL530-HA samples, a 55 wt% solution was applied for molding (in the presence of 2 mol% TPO-L as PI, with regard to the acrylate content of the polymer; note that the samples were dissolved in a larger amount of chloroform 1.4–8 wt%, see Table 1, therefore, excessive solvent was evaporated from the samples, *vide supra*). The vacuum molding was performed at 50 °C. Afterwards, excessive molding solution was removed from the molds, while the base of the microneedle arrays was filled with blank AUP-PCL530-HA solutions (55 wt%) and UV-A irradiated (I = 7.5 mW/cm^2) for 10 minutes to gain shape fidelity. Subsequently, the samples were removed from the molds and air-dried prior to application.

1.4.3. Casting of AUP-PCL and PCL based polymer films

The general film-casting procedure of AUP-PCL530-HA samples was described under *Swelling, gel fraction experiments* (*vide supra*) section. Hereby, the different compositions listed in Table 1 were crosslinked for the thermal evaluation of the compositions. To perform film casting of PCL 80 kg/mol samples, different PCL 80 kg/mol-based solutions (Table 1) were prepared and transferred between two glass plates separated with a 1 mm silicone spacer. Prior to film casting, the excessive solvent (5–25 ml) was evaporated from the plates. Upon achieving shape fidelity of the different PCL-based compositions, the samples were vacuum dried at 50 °C.

1.4.4. Determination of thermal properties via differential scanning calorimetry (DSC) and thermogravimetric analysis (TGA)

Thermogravimetric analysis was performed on a TGA Q50 (TA Instruments) at a heating rate of 10 °C/min from 35 °C up to 750 °C on 10 mg sample amounts. The degradation temperature was determined as the value measured at 5% weight loss. Samples were weighed in a platinum pan under a nitrogen flow (60 ml/min) and the balance was stabilized at a nitrogen flow of 40 ml/min.

To determine the thermal transitions in the polymer compositions (glass transition, T_g, crystallization, T_c and melting temperature, T_m), differential scanning calorimetry (DSC, Q2000, TA Instruments, RSC90 cooler, Zellik, Belgium) measurements were performed on 5 mg sample amounts. The samples were measured in T_{zero} pans, while an empty pan was used as reference, and all the measurements were performed under nitrogen flow (50 ml/min). Two heating cycles were executed, with a cooling cycle in between. The first cycle was to erase the thermal history of the samples, according to the following method: (1) Equilibrate at 0 °C. (2) First heating cycle at a heating rate of 10 °C/min up to 100 °C. (3) Isothermal for 5 min at 100 °C. (4) Cooling cycle at a cooling rate of 10 °C/min to −90 °C. (5) Isothermal for 5 min at −90 °C. (6) Second heating cycle at a heating rate of 10 °C/min up to 250 °C. Isothermal for 5 min at 250 °C. The gained data both

from the TGA and DSC measurements were analyzed in the TA Universal Analysis software.

1.4.5. Compression testing of MN arrays

To determine the mechanical properties, compression testing was performed on a universal testing machine (Tinius Olsen) equipped with a 25 N load cell at room temperature (De Decker et al., 2023c). The preload was set at 0.1 N, and the speed of the compression was set at 0.5 mm/min until 20 N load was reached. The load as a function of displacement was evaluated. Wei-Ze et al showed that 7 N is considered as thumb insertion force on skin samples upon applying microneedle arrays. Therefore, the goal was to identify, if the fabricated MN arrays can withstand 7 N compression force (Wei-Ze et al., 2010).

1.4.6. Swelling and gel fraction of the MN array formulations

To determine the swelling capacity and gel fraction of photo-crosslinked AUP-PCL530-HA and PCL 80 kg/mol in distilled water, prior to the drug release studies, first, a 1 mm thick sheet of AUP-PCL-HA was film-casted, as described in the section *Swelling and gel fraction experiments* (*vide supra*). Subsequently, disks of 7 mm diameter were punched out from the crosslinked AUP-PCL530-HA sheet. The AUP-PCL530-HA disks and untreated PCL 80 kg/mol samples were dried under vacuum. The dry PCL-based samples were weighed (w_{d1}) and afterwards incubated in distilled water for 72 hours at 37 °C and weighed (w_s). Finally, the swollen samples were vacuum dried and weighed (w_{d2}). The swelling degree and gel fraction were determined with Eqs. (3)–(4).

1.4.7. Drug release studies

Prior to the UV–VIS measurements (Shimadzu UV1900I) during the drug release study, the UV–VIS spectrum of hydrocortisone was evaluated to assess the λ_{max} of the compound. The absorbance spectrum of HC as a function of wavenumber (nm) was recorded. The λ_{max} value was used for further measurements. In addition, the UV–VIS spectrum of Brij®35 was recorded, in order to confirm that the additive did not exhibit an interfering UV–VIS signal with the HC.

To evaluate the drug release profile of the fabricated MN arrays, four samples of each sample type were evaluated ($n = 4$). The samples were incubated in 1 ml PBS at 37 °C. Upon sampling, the full volume (1 ml) of PBS was removed and refreshed to gain information on the cumulative release profiles. Sampling was performed after 0, 1, 2, 4, 6, 24 hours and after 2, 3, 5, 7, 10, 14, 17, 21 days. Table 2 gives information on the sample contents and the amount of HC and/or Brij®35 encapsulated. The collected samples were analyzed via UV–VIS spectroscopy (Shimadzu UV1900I), in photometric mode investigating the absorbance at $\lambda = 251$ nm.

1.4.8. Morphological evaluation of MN arrays

To study the effect of the drug release testing, compression testing and skin insertion on the morphology of the molded MN arrays, scanning electron microscopy (SEM, JEOL JCM-7000) was exploited. Prior to visualization, the samples were vacuum dried at 50 °C to remove all solvent residues and gold coated (Automatic Sputter Coater K550X with a RV3 two stage rotary vane pump) to maintain conductivity of the samples. The visualization was performed in secondary electron (SEC) mode.

1.5. Histological evaluation of skin insertion efficiency

Skin for *ex vivo* penetration experiments were procured as residuary material after surgery, i.e., subcutaneous mastectomy in a transmale patient concerning gender affirming surgery. Oral and written informed consent were obtained from the patient prior to tissue procurement. AUP-PCL530-HA and PCL 80 kg/mol MN arrays were tested, both empty and drug-embedded. The skin sample was carefully dissected after procurement, and both glandular and fatty tissue were removed up to the dermal layer. The *ex vivo* skin sample was then stretched using surgical instruments and subsequently pierced thrice with the same sample using thumb force. The array was then removed and stored for integrity evaluation. The tissue was fixated in a 10% formol solution. Automatic Hematoxylin and Eosin staining of the paraffin slices was used (T181 Tissue-Tek Prisma Plus, Sakura Finetek, Antwerp, Belgium). Skin penetration capacity was assessed by evaluating the skins' epidermal layer using optical microscopy (Axio Lab A1, Zeiss, Jena, Germany) on the 3 µm thick histological slices. The analysis of transdermal penetration characteristics for the formed microneedle cavities was conducted using analytical histological software NDP View 2. This evaluation focused on measuring both the depth of microneedle penetration, the width of epidermal separation at the microneedle cavity's base and the distance between two microneedle cavities on average.

Table 2. List of the developed PCL-based MN precursor formulations utilized during characterization of the MN arrays, drug release studies and skin penetration evaluation. As not all types of arrays were evaluated in all studies, each subsection defines the utilized sample types throughout the manuscript utilizing the samples codes. The effectively encapsulated HC amounts were determined after the molding procedure.

PCL type	Hydrocortisone (HC) content (mg/mg polymer)	Effectively encapsulated HC (mg/MN array)	Brij®35 content (µl/mg polymer)	Code name PCL-type +
PCL 80 kg/mol	–	–	–	Control
	50/500	2.98 ± 0.66	–	HC
	–	–	50/500	Brij®35
	50/500	1.64 ± 0.39	50/500	HC + Brij®35
AUP-PCL530-HA	–	–	–	Control
	50/500	1.15 ± 0.21	–	HC
	–	–	50/500	Brij®35
	50/500	0.95 ± 0.10	50/500	HC + Brij®35
	125/500	1.02 ± 0.35	–	2.5×, HC
	125/500	1.13 ± 0.14	50/500	2.5 section, HC + Brij®35
	250/500	2.78 ± 0.43	–	5 section, HC
	250/500	1.98 ± 0.30	50/500	5 section, HC + Brij®35

1.6. Statistical analysis

At least $n = 3$ replicates were applied in all experiments, presented as mean ± standard deviation. GraphPad Prism 8.0.2. was used to perform one-way ANOVA and student's *t*-tests, unless otherwise stated. Results were statistically significant in case $P < .05$.

2. Results and discussion

2.1. Synthesis of acrylate-endcapped urethane-based poly(ε-caprolactone)

2.1.1. Physico-chemical characterization of the photo-crosslinkable PCL

Physico-chemical characterization of the acrylate-endcapped urethane-based precursor was performed to verify successful synthesis. The ^{1}H-NMR spectrum of AUP-PCL530-HA confirmed that the acrylation of the PCL-diol was sufficient, with a final acrylate concentration of 2.17 mmol/g AUP-PCL530-HA (based on Eq. (1), see Figure 2 (A)). The molar mass was determined based on the NMR spectrum and Eq. (2) and was found to be 2600 g/mol, which was in line with previous reports (Vermoesen et al., 2023). Subsequent to the synthesis, the swelling degree of the product was evaluated in chloroform, based on Eq. (3), which showed a swelling capacity of 2.21 ± 0.06. The gel fraction was 94.55 ± 2.11%, based on Eq. (4), which implies efficient crosslinking (Figure 2 (B)).

2.2. Evaluation of PCL-based MN arrays

2.2.1. Physical evaluation of the MN arrays

2.2.1.1. Swelling and gel fraction determination of PCL-based polymers in aqueous media. As the drug release takes place in aqueous conditions in the skin, the swelling behavior and gel fraction values of crosslinked AUP-PCL530-HA and solid PCL 80 kg/mol were determined in distilled water at body temperature (37 °C). AUP-PCL530-HA showed a swelling degree of 1.07 ± 0.03, while PCL 80 kg/mol showed a swelling degree of 1.01 ± 0.00 (Figure 3(A)). This implied that neither of these PCL-based materials showed a significant swelling in aqueous conditions.

The gel fraction values suggested, that in case of AUP-PCL530-HA, the obtained values were not significantly different from the ones measured in chloroform (94.18 ± 0.53% in distilled water, Figure 3(B), vs 94.55 ± 2.11% in chloroform, Figure 2(B)), whereas for PCL 80 kg/mol, a value of 99.69 ± 0.26% was found (Figure 3(B)). The results implied that the additives incorporated during the synthesis of AUP-PCL530-HA (Vermoesen et al., 2023) (catalysts, unreacted endcapping agent, radical scavengers, such as BHT (Buthylated hydroxytoluene, Safety data sheet - Buthylated hydroxytoluene., n.d), TPP (Triphenylphosphine., n.d), PTZ (Phenotiazine, Safety data sheet - Phenotiazine, Safety Data Sheet., n.d), etc.) leached out upon swelling the AUP polymer in aqueous media, which caused a reduction in the gel fraction values (compared to 100%).

2.2.1.2. Thermal properties of PCL-based polymers. The thermal properties of the PCL-based polymer formulations, as well the model drug (hydrocortisone) and the additive (Brij®35) individually were evaluated via thermogravimetric analysis (TGA) and differential scanning calorimetry (DSC). In case of the AUP-PCL530-HA samples, crosslinked blends were used for the following tests. The extensive list of the blends can be found in Table 2, while Tables 3–4 show the compositions utilized in each measurement along with the gained results.

Table 3 presents the 5% mass loss temperature and onset temperature of the degradation of the different compounds and their blends. The results suggested that the hydrocortisone and Brij®35 exhibited a lower degradation temperature compared to pure PCL 80 kg/mol and AUP-PCL530-HA polymers. The presence of the additives in the PCL-based formulations substantially lowered the degradation temperature of the polymer–additive blends (Mondal et al., 2016), as the degradation temperatures of the additives were lower than

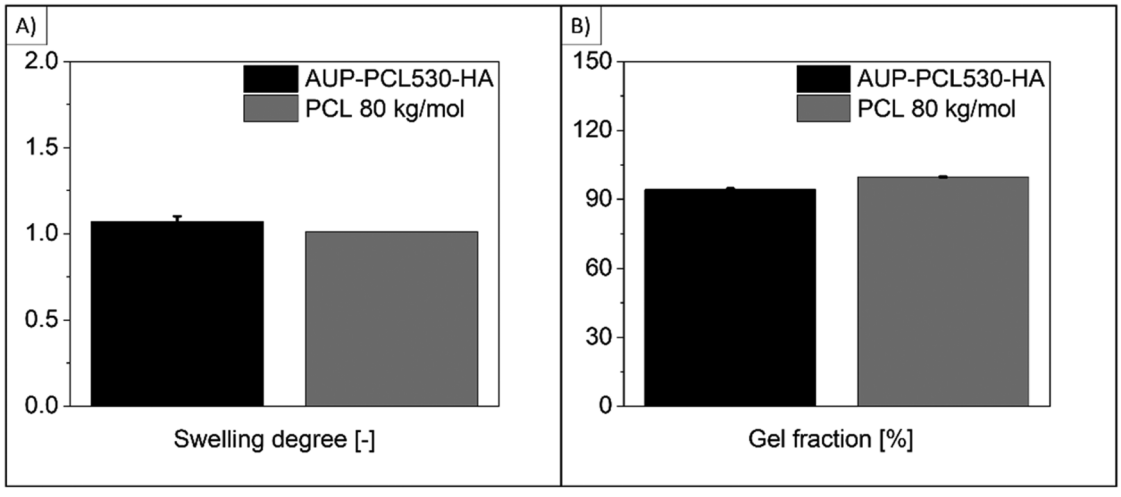

Figure 3. Swelling degree and gel fraction values of AUP-PCL530-HA and PCL 80 kg/mol in aqueous media. (a) suggests that no significant swelling of the PCL-based polymers could be observed in distilled water, which is in line with the hydrophobic nature of PCL. (B) shows a high (>90%) gel fraction for the PCL-based polymers in aqueous media. However, in case of the AUP-PCL530-HA, the leaching out of additives applied during production (O'Neil, 2001) could be observed through the gel fraction decrease.

those of the polymer matrices, especially when considering the 5% weight loss temperatures. Nonetheless, since the degradation temperatures were exceeding the intended application temperature, being body temperature (37 °C), the MNs would not exhibit any signs of degradation during use.

To investigate the thermal properties of the MN blends, DSC measurements were performed. PCL with a molar mass of 80 kg/mol is a semi-crystalline polymer, although it is amorphous when it has a molar mass of 530 g/mol due to the short chains not capable of forming crystalline associations (Mondal et al., 2016).

In case of the PCL 80 kg/mol blends, the goal was to evaluate whether the hydrocortisone or Brij®35 would have a significant effect on the crystallinity and hence, on the drug release profile of the formulations. Upon incorporation of HC into the PCL 80 kg/mol blends, the T_c (from 26 °C to 31 °C) showed a substantial increase, implying that HC crystals within the polymer could act as nucleation sites, increasing the crystallization temperature of the polymer (Van Renterghem et al., 2018). The T_m did not show a substantial difference (increase from 51 °C to 52 °C), although the melting enthalpy (H_m) decreased from 65.7 J/g to 44.6 J/g which suggested a lower degree of crystallinity of PCL, upon incorporating the drug. As the T_m values were situated around 50 °C, hence exceeding body temperature, the PCL 80 kg/mol-based MN arrays were in semi-crystalline state at application temperature. This also applies for the MN arrays supplemented with Brij®35 versus HC + Brij®35.

A second crystallization and melting peak could be observed on the DSC thermogram in case of the blends containing Brij®35 only, which are lower than the T_c and T_m of the PCL 80 kg/mol and Brij®35 (Table 4). This could be the result of the formation of surfactant aggregates or surfactant-polymer aggregates during sample preparation in the precursor solution, and in the dry MN arrays as well. The melting enthalpy of this second peak was significantly lower than the one of the pure PCL, as the Brij®35 content of the samples was only 50 µl/500 mg (corresponding to 0.04 mmol/0.01 mmol) polymer; therefore, the amount of aggregates compared to the full sample mass was limited (Rask et al., 2018). Interestingly, in case of HC + Brij®35 containing formulations, the crystallization and melting peaks in the region of Brij®35 melting were not detectable, although a melting peak at T_m = 167 °C was present, along with a substantially lower melting enthalpy compared to that of pure PCL. The decrease of melting enthalpy, which can be rendered to HC/polymer aggregates was in agreement with the observations in case of the Brij®35 incorporated samples (Brij®35/polymer aggregates). As the T_m was observed at relatively high temperatures in case of the HC + Brij®35 incorporating PCL 80 kg/mol samples, closer to the melting temperature of pure HC (T_m = 225 °C (Khan et al., 2017), it was hypothesized that in a PCL 80 kg/mol/HC/Brij®35 ternary system, the coordination of the Brij®35 to the HC molecules was predominant over its association with PCL 80 kg/mol, resulting in the formation of Brij®35-HC aggregates in the MN systems (Rask et al., 2018; Solaiman et al., 2015; Kapourani et al., 2021). Within the surfactant-drug aggregates, the Brij®35 had a plasticizer effect on the crystalline HC, which resulted in a T_m decrease compared to that of the pure compound (Kapourani et al., 2021).

In case of the AUP-PCL530-HA-based compositions, no crystallization or melting were detectable in the control samples nor in the Brij®35-containing compositions, suggesting that the additive had an excellent miscibility in AUP-PCL530-HA

Table 3. TGA data of the PCL-based polymer compositions applied for the development of the MN arrays.

PCL type	Hydrocortisone (HC) content* (mg/mg polymer)	**Brij®35 content* (µl/mg polymer)**	**5% mass loss temperature (°C)**	**Onset temperature (°C)**
-	50/0	–	256	315
-	–	50/0	236	347
PCL 80 kg/mol	–	–	360	375
	50/500	–	307	373
	–	50/500	301	362
	50/500	50/500	302	371
AUP-PCL530-HA	–	–	297	334
	50/500	–	274	357
	–	50/500	290	336
	50/500	50/500	296	337

*The molar ratios of the HC and Brij®35 are listed in Table 1.

Table 4. Thermal properties of the PCL-based polymer compositions and additives applied for the development of the MN arrays determined via DSC.

PCL type	Hydrocortisone (HC) content (mg/mg polymer)	**Brij®35 content (µl/mg polymer)**	Molding solvent	**T_c [°C]**	**T_{cp} [°C]**	**H_c [J/G]**	**T_g [°C]**	**T_m [°C]**	**T_{mp} [°C]**	**H_m [J/G]**
-	50/0	–	-	–	–	–	–	224.7	225.1	131.5
-	–	50/0	-	19.4	16.2	130.7	–	32.7	42.8	112.3
PCL 80 kg/mol	–	–	Chloroform	25.8	18.5	59.5	−62.5	50.9	55.5	64.7
	50/500	–		30.7	26.7	56.2	−61.3	51.5	55.4	44.6
	–	50/500		35.5	27.1	48.0	−59.1	51.2	55.6	39.4
				7.7*	−0.1*	7.3*	-*	23.5*	36.5*	9.6*
	50/500	50/500		35.0	30.8	51.9	−62.4	52.6	55.1	52.2
				–	–	–	–	140.7**	166.9**	4.0**
AUP-PCL530-HA	–	–	Acetone	–	–	–	–	–	–	–
	50/500	–		–	–	–	–	–	–	–
				–	–	–	–	166.2**	198.7**	6.6**
	–	50/500		–	–	–	–	–	–	–
				–	–	–	–	–	–	–
	50/500	50/500		–	–	–	–	–	–	–
				–	–	–	–	198.3**	211.7**	0.1**

*Second melting/crystallization peak appearance in the region of melting/crystallization of pure Brij®35 compound.
**Second melting/crystallization peak appearance in the region of melting/crystallization of pure hydrocortisone compound.

showing no specific aggregation profile (Gainanova et al., 2006). In case of the AUP-PCL530-HA samples supplemented with HC, a melting peak was observed corresponding with a T_m = 166 °C—although lower than the melting temperature of the pure HC compound (T_m = 225 °C; Khan et al., 2017)—along with a considerably lower melting enthalpy (H_m). This implied partial crystalline phase separation of the drug molecule from the AUP-PCL530-HA matrix (Rask et al., 2018). In agreement with the previous observations for the PCL 80 kg/mol matrix, upon supplementing AUP-PCL530-HA with the combination of HC + Brij®35, a minor melting peak close to the melting region of the pure Brij®35 (T_m = 33 °C) was observable at T_m = 35 °C, with a H_m = 0.14 J/g. Upon supplementation of the HC containing AUP-PCL530-HA samples with Brij®35, the surfactant lowered the crystallinity of the drug molecules (Claeys et al., 2015), creating an amorphous distribution of the HC in the matrix, while forming Brij®35 aggregates, which could be observed in the DSC thermogram (Gainanova et al., 2006; Qi et al., 2013; Kapourani et al., 2021). Therefore, it was hypothesized that the second melting peak in the DSC thermograms of AUP-PCL530-HA, supplemented with HC + Brij®35 was resulting from the presence of Brij®35 aggregates in the blends. On the contrary, the appearance of a second melting peak in the PCL 80 kg/mol samples' thermograms was in the HC region, upon utilizing HC + Brij®35 in the blend suggesting the partial crystallization of HC. Costa et al have observed a similar phenomenon, namely that plasticizers (herein Brij®35) influence the crystallization of crystalline drug molecules in polymer matrices, which can act as nucleation site for crystallization (Costa et al., 2016). However, these interactions depend on the properties of the polymer/surfactant/drug ternary systems.

2.2.2. Mechanical properties of the micro-molded arrays

Park et al developed a standard method for evaluating the mechanical properties and skin insertion efficiency of PLA, PGA and PLGA MN arrays which was extended to all MN prototypes ever since (Park et al., 2005, 2006). The mechanical evaluation of the herein developed PCL-based MN arrays was executed with the method mentioned above. The load (N) was monitored as a function of displacement for the PCL-based MN arrays (n = 4). The data showed that the microneedles were still intact at a 7 N load (Figure 4), which is corresponding with the hand-pressing load on the arrays upon application on the treated area ($F_i \cong 7$N, Figure 4(A and B) (Wei-Ze et al., 2010). The presence of HC and/or Brij®35) did not show a pronounced effect on the macro-mechanical properties of the MN arrays at 7 N insertion force. However, above 15 N load, in case of the AUP-PCL530-HA arrays, while above 8–10 N in case of the PCL 80 kg/mol samples, the mechanical integrity of the MN arrays was compromised. The PCL 80 kg/mol needles showed an irreversible bending of the needles upon compression, although the majority of the AUP-PCL530-HA needles remained intact after compression. Thanks to the amorphous state of the PCL530, the structures maintained outstanding flexibility.

However, the DSC results suggested (Table 4), that in case of the AUP-PCL530-HA HC loaded sample, partial crystallization of the HC was observable, yet in HC and Brij®35 loaded

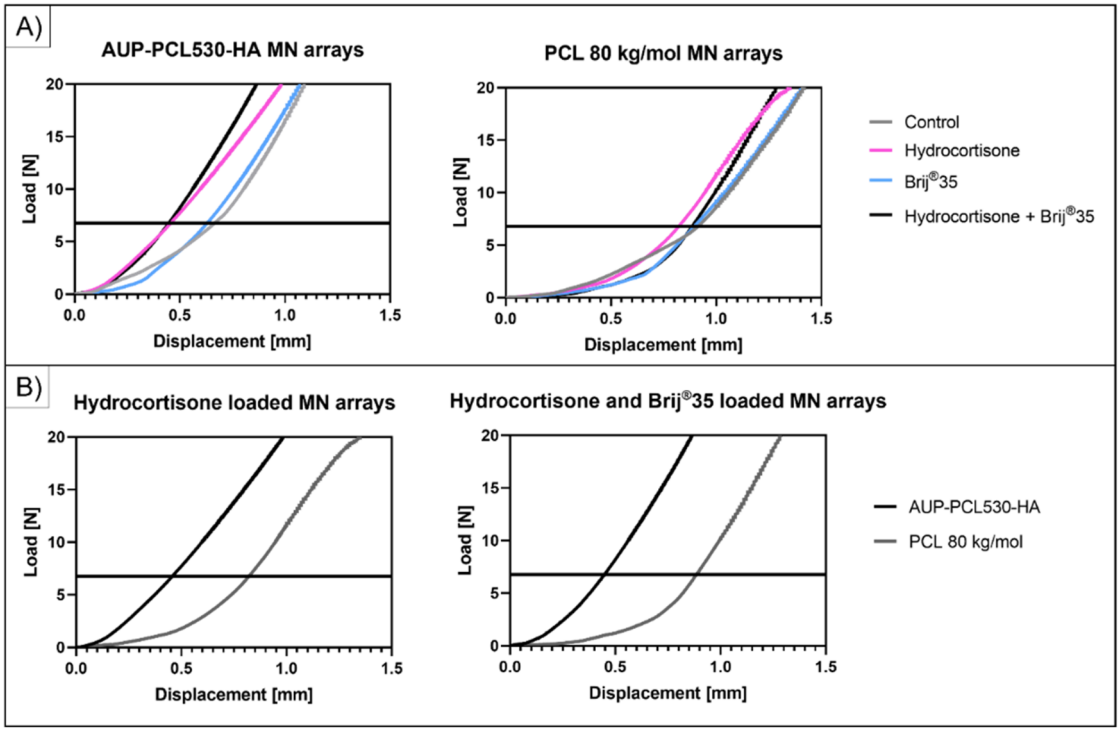

Figure 4. Mechanical evaluation of the PCL-based MN arrays exploiting compression testing. Both the AUP-PCL530-HA and PCL 80 kg/mol MN arrays could withstand the 7 N compression force limit, which is considered the hand-pressing insertion force. The AUP-PCL530-HA-based MN arrays showed excellent compression resistance up to 15-20 N load, whereas the PCL 80 kg/mol-based MN arrays could withstand 8–10 N load at 0.5 mm/min compression speed. The presence of HC and/or brij®35 did not show a pronounced effect on the mechanical properties of the MN arrays.

samples, no crystallization peak of the HC was detectable. SEM micrographs showed inhomogeneities across the needle structures of both samples (Figure 8 – HC loaded, Figure S2 HC + Brij®35 loaded). Generally, the presence of crystalline additives, which can interface with the polymer matrices, can lead to the presence of nucleation sites of fracture (Hardy et al., 2006). While the AUP-PCL530-HA MN arrays encapsulating HC did not show failure of the needle structures, in case of the structures of the MNs incorporating HC + Brij®35, needle failure and fracture were observable, due to the plasticizer effect of the surfactant on the polymer matrix (Yavuz et al., 2020; Heng and Wan, 1990; Johnson et al., 2022) (Figure S2).

2.2.3. Drug-release profile of the different PCL 80 kg/mol and AUP-PCL530-HA MN-arrays

The aim of the study was to develop a MN array, which is characterized by an extended controlled corticoid release profile over 21 days. Multiple types of corticosteroids exist with different potencies toward HTS treatment. For corticoid injection, triamcinolone acetonide (TAC, 434.5 g/mol) and betamethasone (BM, 392.5 g/mol) are most commonly used. HC (362.5 g/mol), being characterized by a similar molar mass as compared to TAC and BM, was used for the embedding process. Given the similar molar mass of these products, a similar distribution pattern could be expected. Given the hydrophobic nature of the PCL-based polymers, supported by the swelling data (Figure 3(A)), which suggested that neither the AUP-PCL530-HA (1.07 ± 0.03), nor the PCL 80 kg/mol (1.01 ± 0.00) showed significant swelling in aqueous media, upon homogeneous drug distribution in the MN arrays. Hence, the diffusion of HC upon release from the polymer matrices could be described by the Fickian diffusion model (Park et al., 2006).

Prior to the evaluation of the drug release profile, the UV–VIS spectrum of the pure HC and Brij®35 was recorded (Figure S1). Brij®35 exhibited no overlapping signals with HC in the UV–VIS region, rendering UV–VIS spectroscopy suitable for evaluating drug release.

Figure 5(A) illustrates the release profile of HC from the AUP-PCL530-HA (left) and PCL 80 kg/mol (right) MN arrays. MN arrays of pure polymers (control), MN arrays incorporating only HC or Brij®35 versus HC + Brij®35 were evaluated. The composition of the arrays, along with the efficiently encapsulated HC amount/array is listed in Table 2. The HC-incorporating MN arrays showed a continuous HC release up to 21 days in case of the AUP-PCL530-HA arrays (49.6 ± 13.8% of the original drug load, correlating to 0.57 ± 0.10 mg HC), while the PCL 80 kg/mol-based MNs only offered a release for 48 hours (13.6 ± 3.8% of the original drug load, correlating to 0.40 ± 0.09 mg HC). Orozco-Castellanos et al reported similar values for HC release from PCL-based polymers (Orozco-Castellanos et al., 2011). At pH 7.4, they reported a cumulative release of HC ranging from about 13%–45% based on the amount of amorphous polymer phase in the PCL-based matrices. The more extended the amorphous region was, the more pronounced the HC release (Orozco-Castellanos et al., 2011). Similarly, it could be stated that the AUP-PCL530-HA amorphous polymer-based MN arrays outperformed the semi-crystalline PCL 80 kg/mol-based ones (Heng and Wan, 1990). The observations were in line with the study from Izumikawa et al. focusing on the drug release of crystalline progesterone from amorphous and crystalline PLLA microspheres, which proved that an amorphous matrix significantly increased the drug release efficiency from the polymeric carrier (Izumikawa et al., n.d). The AUP-PCL530-HA hydrocortisone-loaded MN arrays provided a 42.5% higher HC release over a 10-times longer period. This implied an extended, sustained release of the corticosteroid in the hypertrophic scars.

In order to improve the drug release efficiency, the HC-loaded MN arrays were supplemented with Brij®35, a non-ionic surfactant (Table 2, Figure 5(A and B)). Surfactants can provide a significant increase in drug release rates, which has been exploited in pharmaceutical formulations since the 1980s (Heng and Wan, 1990). In line with the state-of-the-art, a drastic increase in the release profile could be observed in case of both polymer-based MN arrays, as the Brij®35 could act as plasticizer in the polymer matrices and increased the mobility of the PCL chains (Yavuz et al., 2020; Heng and Wan, 1990; Johnson et al., 2022). The PCL 80 kg/mol-based HC-loaded MN arrays only offered a steady release of 0.40 ± 0.09 mg HC for 48 hours, while the Brij®35 supplemented ones provided an extended release up to 7 days and 23.9 ± 14.7% of the original drug load, correlating to 0.39 ± 0.09 mg HC. The results suggested that the incorporation of Brij®35 could extend the release duration with more than 3-fold, although the released amount of HC was not significantly different from the HC-loaded arrays ($p = 0.88$), as a lower drug load was achieved with the combination of HC + Brij®35 (1.64 ± 0.39 mg vs. 2.98 ± 0.66 mg in case of the HC-loaded MN arrays). In case of the AUP-PCL530-HA MN arrays, a similar trend became apparent. Albeit the HC-loaded MNs could encapsulate 1.15 ± 0.21 mg of drug, and release 0.57 ± 0.10 mg over 21 days, the HC + Brij®35 supplemented MNs could incorporate 0.95 ± 0.10 mg drug, while offering a sustained release of 0.70 ± 0.10 mg HC, which correlated to 22% increase in the delivered drug amount over the same period of time, although the results did not show a significant difference ($p = 0.12$). Similarly, Yavuz et al. reported an increased release (with approximately 20%) of the hormone levonorgestrel and an extension of the efficient drug delivery window from 40 to 50 days (20% increase) in case of silk fibroin MN arrays (Yavuz et al., 2020). Based on the results, the authors suggest applying HC in the MN arrays without incorporating Brij®35 upon the fabrication of the AUP-PCL530-HA arrays.

In our previous study, De Decker et al. successfully applied 0.89 mg/cm^2 corticosteroid-loaded hyaluronic acid patches on hypertrophic wounds in a 4-month pilot study (De Decker et al., 2023c). However, the HA-based MN arrays applied in the pilot study consisted of 320 MNs, whereas the currently developed MN arrays consisted of 36 individual MNs. To this end, upon changing the MN array design to that of De Decker et al., a cumulative drug release of 5.07 ± 0.89 mg/cm^2 could be foreseen in case of the HC loaded AUP-PCL530-HA arrays.

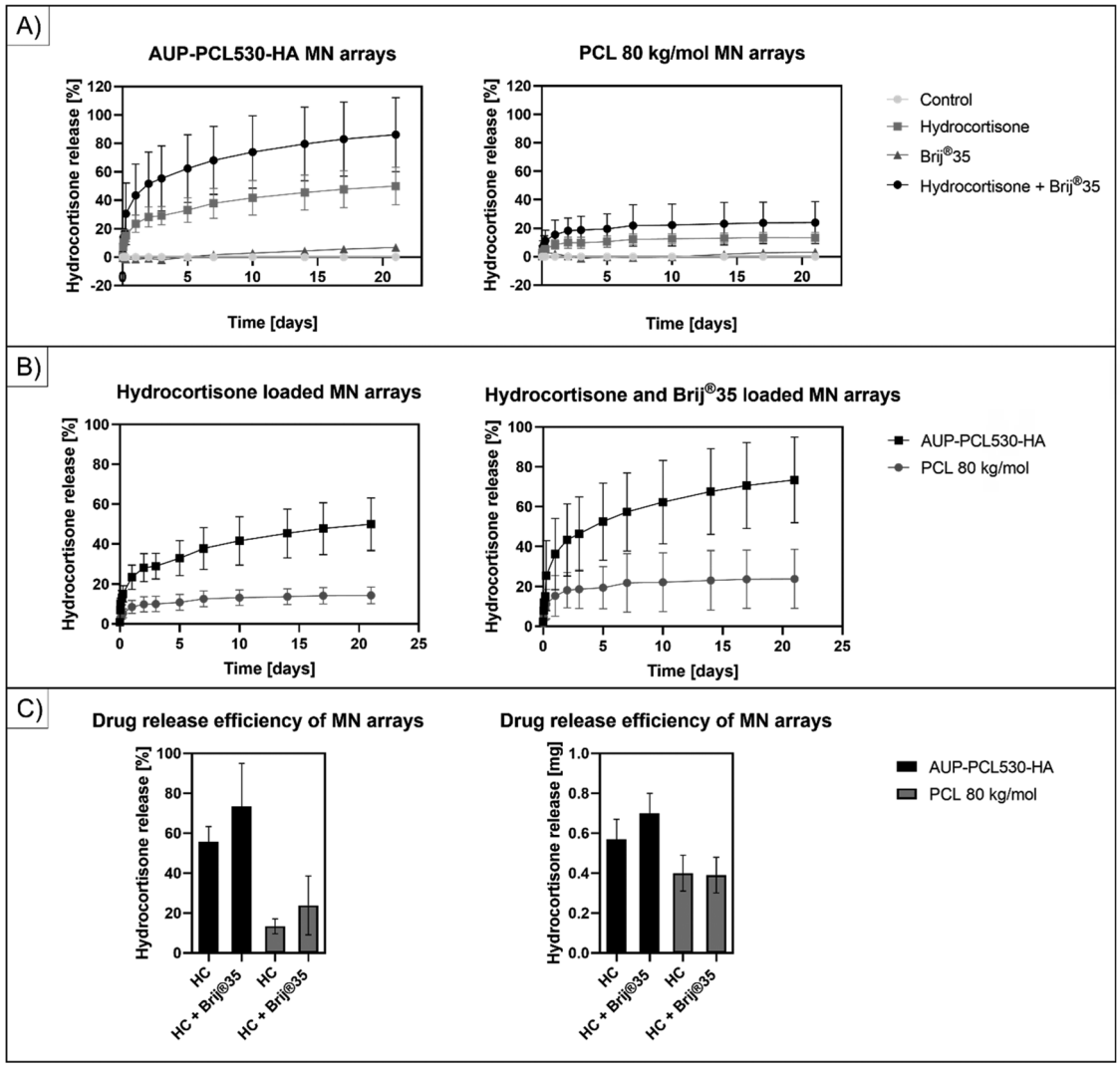

Figure 5. Illustration of the extended drug release profile of hydrocortisone from the different PCL-based MN arrays. (a) shows the cumulative HC release from the control, HC, brij®35 and HC + brij®35 containing MN arrays. The composition of the MN arrays can be found in Table 2. A significant release increase could be observed upon utilizing brij®35 as release enhancer in combination with HC compared to the HC-containing samples for both AUP-PCL530-HA and PCL 80 kg/mol MN arrays, while the control and brij®35 containing samples did not show any HC release. (B) shows a substantial increase in the cumulative HC release upon the utilization of AUP-PCL530-HA as polymer matrix contrary to the PCL 80 kg/mol due to the lack of crystallinity in the AUP matrix both for HC and for HC + brij®35 containing MN arrays. The graphs also indicate that while the PCL 80 kg/mol-based MN arrays could provide a sustained HC release for 7 days, upon utilization of AUP-PCL530-HA, the release profile could be extended up to 21 days. (C) shows the cumulative release of HC in percentage as a function of HC load on the left and in milligrams (mg) on the right over 21 days of release. The application of brij®35 did not have a significantly increasing effect on the HC release ($p > .05$).

The standard care applies a drug delivery up to 30 mg/treatment, therefore we aimed to excessively increase the drug load of our MNs. Due to phase separation and enhanced crystallization of the HC molecules during the molding procedure, the maximum loading we could apply was five times higher than in regular MN's (Table 2, Figure 6(A and B)). We have obtained MN arrays with 2.5- and 5-times higher drug encapsulation loading without Brij®35 and in the presence of 50 µl/500 mg polymer Brij®35 load, respectively. The drug release studies were monitored for 10 days (Orozco-Castellanos et al., 2011).

Figure 6 suggests a decrease in the drug release efficiency upon increasing the drug load in the AUP-PCL530-HA MN arrays during 10 days of release. In case of only HC loaded AUP-PCL530-HA MN arrays, upon increasing the drug content 2.5 times (125 mg/500 mg polymer load), 1.02 ± 0.35 mg HC was incorporated, while 0.19 ± 0.07 mg was released, while upon increasing the drug content 5 times (250 mg/500 mg polymer load), 2.78 ± 0.43 mg was encapsulated, yet only 0.24 ± 0.04 mg HC was released. Upon supplementing the same setup with 50 µl/500 mg polymer Brij®35, in case of the original drug load, 0.95 ± 0.10 mg HC was incorporated in the MNs and 0.59 ± 0.07 mg was released, while at a 2.5x loading, 1.13 ± 0.14 mg HC was encapsulated and 0.17 ± 0.02 mg was released, and upon a 5x HC loading, 1.98 ± 0.30 mg was incorporated, while only 0.37 ± 0.06 mg was released. Therefore, it was concluded that the same trend could be observed, upon increasing the crystalline HC load in the MN arrays. More specifically, the release efficiency deteriorated, even upon the application of Brij®35 as a release enhancer. This could be due to the limited solubility of the crystalline HC in the AUP polymer, which led to more pronounced crystallization and phase separation of the drug molecules.

2.2.4. Morphological analysis of the vacuum-molded MN arrays

The morphological evaluation of the micromoulded MN arrays was performed via SEM measurements. Figure 7 shows the comparison between the morphology of AUP-PCL530-HA- and PCL 80 kg/mol-based MN arrays subsequent to drug release. The upper row indicates the control samples, while the center depicts the HC loaded and the bottom row the HC + Brij®35 loaded ones. The SEM micrographs were in line with the DSC results, which suggested minor aggregation of the HC and Brij®35 compounds in the MN arrays, which led to an increased surface roughness.

Figure 8 demonstrates the morphology changes of the HC loaded AUP-PCL530-HA and PCL 80 kg/mol MN arrays. The top row shows the control samples, a more pronounced phase separation of the drug is visible in the AUP-PCL530-HA arrays compared to the PCL 80 kg/mol ones, in line with the DSC results. Figure 8 showcases the needles following drug release, including the removal of the HC crystals from the AUP-PCL530-HA, while the PCL 80 kg/mol arrays did not show a substantial morphology change subsequent to drug release. The lack of morphology change of the PCL 80 kg/mol MNs originated from the superior miscibility of HC and PCL 80 kg/mol, in agreement with the DSC results (Table 4, no phase separation observed in the thermograms). The third row shows the effect of the compression tests on the MN structures. The AUP-PCL530-HA remained intact, while the PCL 80 kg/mol ones suffered permanent morphology deterioration. Finally, the bottom row demonstrates the HC loaded MNs following *ex vivo* skin insertion. In line with the MNs after compression testing, AUP-PCL530-HA stayed intact, while the PCL 80 kg/mol ones suffered severe morphology deterioration.

Figure S2 demonstrates the effect of the HC and Brij®35 on MNs subsequent to compression testing. Compared to the control and HC containing MNs, the mechanical properties of the arrays deteriorated upon applying Brij®35 in the needles, which was indicated by the ruptures in both the AUP-PCL530-HA and PCL 80 kg/mol needles. As Brij®35 did not significantly affect the drug release profile of the AUP-PCL530-HA arrays, yet had a negative impact on their mechanical properties, its application is not advised in the system.

2.3. Ex vivo clinical application of PCL-based MN arrays

As the MN arrays incorporating HC + Brij®35 showed ruptures upon compression testing, the *ex vivo* skin insertion studies were carried out with control and HC loaded MN arrays. Figure 9 shows the microscopic histological evaluation of the successful skin piercing capabilities of the drug-embedded AUP-PCL530-HA MN, which was illustrated by complete epidermal penetration and indentation of the papillary dermis. The control AUP-PCL530-HA MN showed a similar pyramidical shaped penetration pattern with a regular distance interval. The penetration pattern of both control and drug embedded PCL 80 kg/mol microneedles showed a regular indentation interval on the stratum corneum but did not show adequate and frequent penetrative epidermal cavities, illustrating that these microneedles did not achieve reliable skin penetration. Analysis post-insertion showed structural disintegration of the PCL 80 kg/mol microneedle patches. Figure 10 illustrates the untreated control, with the skin from the same patient being utilized for both histological evaluations. This figure shows the absence of epidermo-dermal penetration cavities. Additionally,

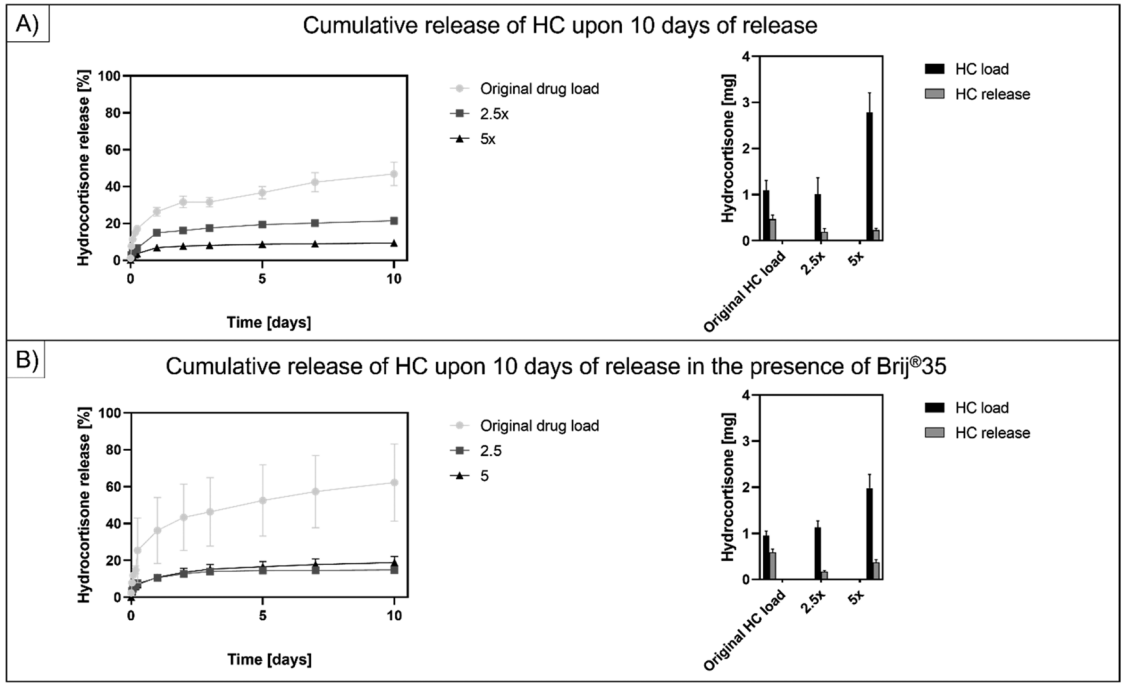

Figure 6. Cumulative release of HC for 10 days. (a) shows the release profile and cumulative release of HC at 50 mg/500 mg polymer load, 125 mg/500 mg polymer load and 250 mg/500 mg polymer load. (B) shows the release profile and cumulative release of HC at 50 mg/500 mg polymer load, 125 mg/500 mg polymer load and 250 mg/500 mg polymer load in the presence of 50 µl/500 mg polymer brij®35 content. The results suggested a decrease in the drug release efficiency upon increasing the drug load in the AUP-PCL530-HA MN arrays.

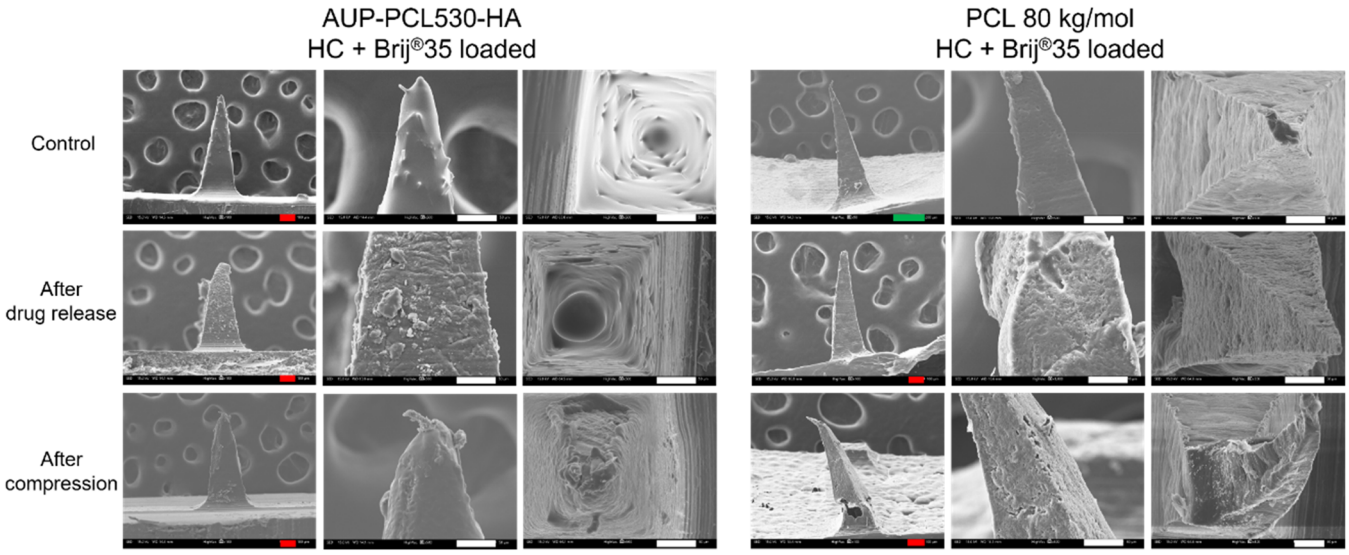

Figure 7. Scanning electron microscopy (SEM) micrographs of AUP-PCL530-HA and PCL 80 kg/mol MN arrays. The top row represents the control, the Middle row the HC loaded and the bottom row the HC + brij®35 loaded MN arrays in side- and top view subsequent to the drug release studies. The incorporation of HC in the MN arrays led to an increased surface roughness of the MNs, due to the partial phase separation between the HC and the PCLs, which induced the crystallization of HC within the MNs. The incorporation of HC + brij®35 in the MN arrays led to an even higher surface roughness of the MNs due to the phase separation occurring between the HC + brij®35 and the PCLs, which was more pronounced in case of the PCL 80 kg/mol arrays. The scale bars refer to the following lengths: green – 200 µm, red – 100 µm, white – 50 µm, blue – 10 µm.

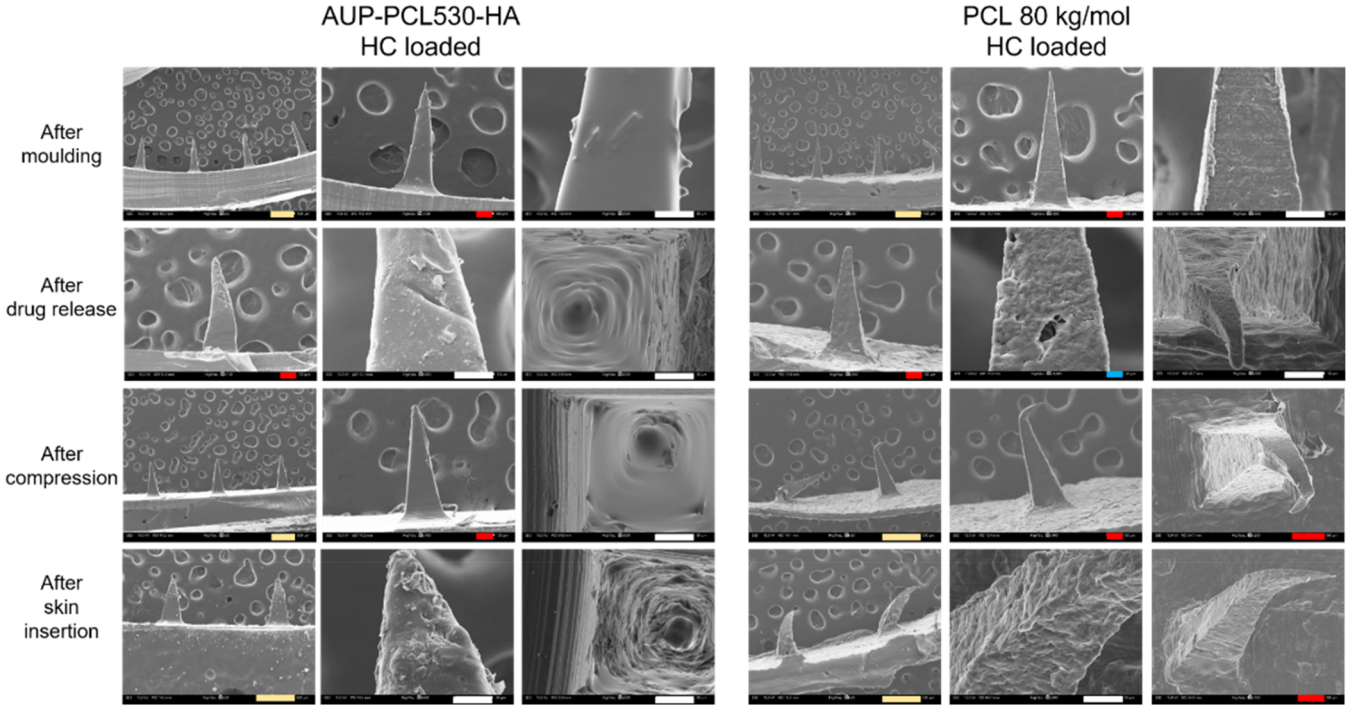

Figure 8. Scanning electron microscopy (SEM) micrographs of AUP-PCL530-HA and PCL 80 kg/mol MN arrays. The top row represents the HC loaded MN arrays after molding, the second row after drug release, the third row after compression testing, and the bottom row following *ex vivo* skin insertion. It should be noted that the phase separation of HC was more pronounced in the AUP-PCL530-HA arrays. Following drug release, the crystals have dissolved from the needles. Moreover, the AUP-PCL530-HA arrays stayed intact subsequent to compression and skin insertion, in contrast with the PCL 80 kg/mol arrays, which permanently deteriorated upon exerting mechanical stress. The scale bars refer to the following lengths: green – 200 µm, red – 100 µm, white – 50 µm, blue – 10 µm.

transdermal penetration characteristics were assessed. The dimensions of the microneedle cavities ($n = 30$) were studied with analytical software, specifically the histological assessment program NDP View 2. Our comprehensive analysis reveiled a dermal penetration depth of 307.14 ± 58.06 µm. The width of the epidermal separation at the base of the microneedle cavity corresponds with a 72.21 ± 13.32 µm. Between two microneedle cavities, there is epidermal interspacing of 250.86 ± 36.56 µm. These quantitative measures serve as significant indicators of the microneedles' proficiency in breaching the skin barrier, thereby enabling the effective intradermal delivery of medication.

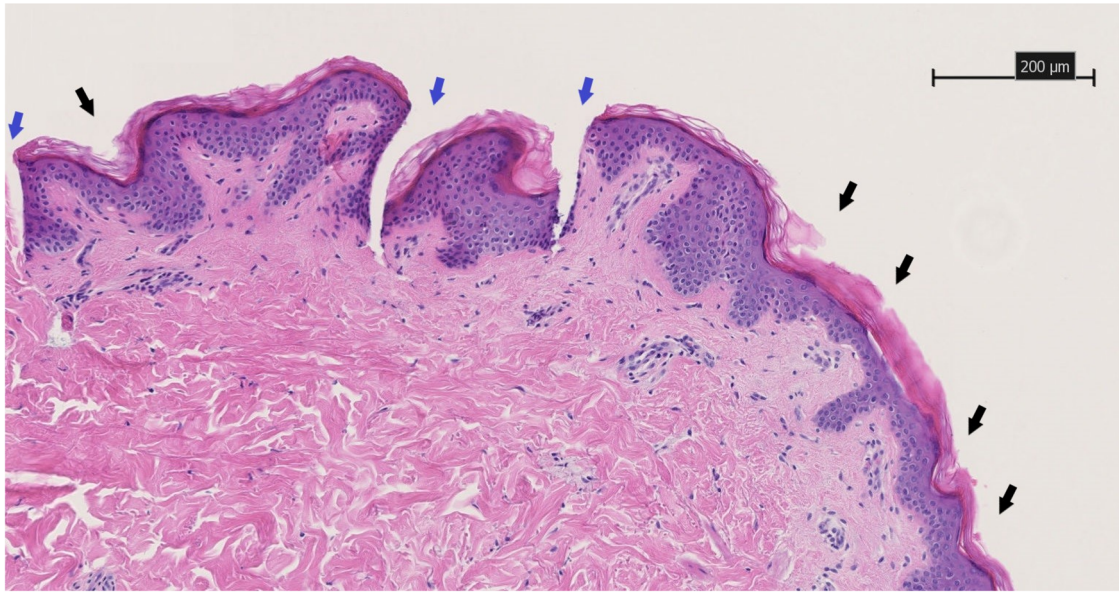

Figure 9. HE-stained 3 µm thick histological slice showing the skin piercing capability of the drug-embedded AUP-PCL530-HA MN. Black arrows show regular indentations of the epidermal layer and blue arrows show the pyramidical shaped penetration cavity through the epidermal layer toward the deeper dermal layer. Both are sequelae of microneedle application. The scale bar represents 200 µm. Magnification is 10x.

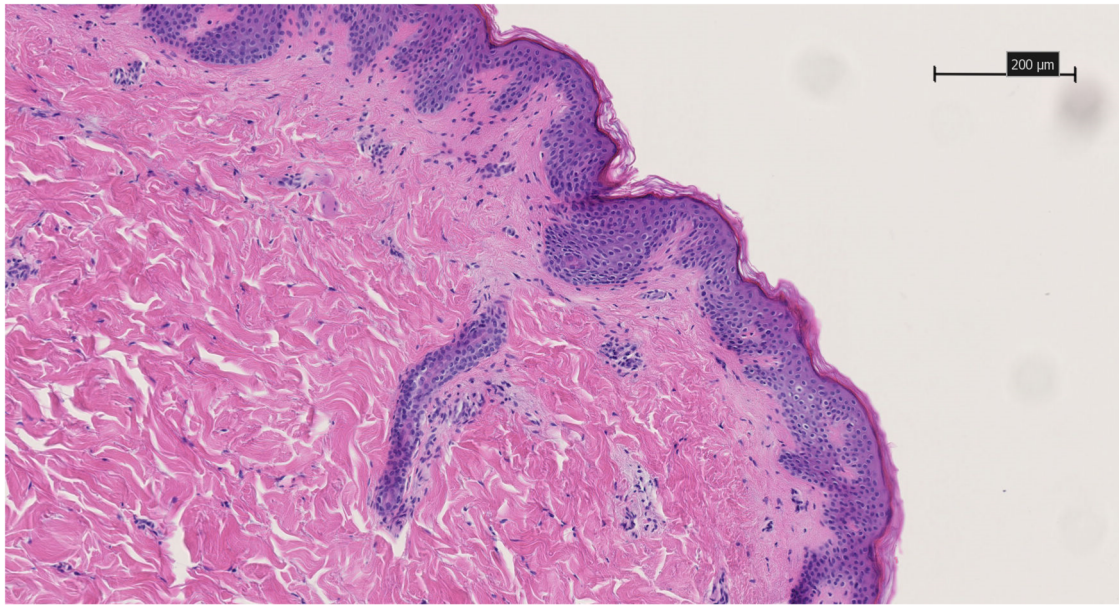

Figure 10. HE-stained 3 µm thick histological slice of the control specimen that did not receive microneedle treatment. The scale bar represents 200 µm. Magnification is 10x.

3. Conclusion

Different AUP-PCL530-HA MN arrays were developed which support the sustained drug release of hydrocortisone toward hypertrophic scar treatment. PCL 80 kg/mol-based MN arrays were fabricated in the same manner, as a benchmark for the novel compositions. The AUP-PCL530-HA MN arrays showed superior mechanical properties and remained intact upon a 15 N load compression, which exceeded the requirement of 7 N load bearing for efficient skin penetration, while the PCL 80 kg/mol arrays deteriorated irreversibly upon exerting 8-10 N load. The thermal analysis of the MN arrays highlighted that the AUP-PCL530-HA polymer was amorphous, while the PCL 80 kg/mol was semi-crystalline which had an effect on the drug release profiles of the MN arrays. The AUP-PCL530-HA-based MN arrays provided a 42.5% higher and 3 times longer drug release compared to the PCL 80 kg/mol-based arrays. Upon incorporation of Brij®35 as a release enhancer, no significant increase was observed for the HC release in case of the AUP-PCL530-HA-based MN arrays during 21 days of sustained release. Finally, the AUP-PCL530-HA-based MN arrays incorporating HC sufficiently penetrated the stratum corneum of *ex vivo* skin samples, while the PCL 80 kg/mol-based arrays did not provide adequate penetration.

Acknowledgements

The authors would like to thank Evelien Vermoesen for the help with regard to the AUP-PCL synthesis. The authors would additionally like to thank Irem Kaya for preparing the histological slices and for providing technical support for the histological evaluation.

Disclosure of interest

Sandra Van Vlierberghe is a co-founder of the companies BIO INX BV and 4Tissue BV, but the author declares to have no known financial interest that could have appeared to influence the work reported in this paper. The other authors declare to have no competing financial or commercial interest or personal relationship that could have appeared to influence the work reported in this manuscript.

Ethical approval

This study did not include treatment of human participants. The collection of and testing on ex vivo human skin was approved by the Ethical Committee of the Ghent University Hospital on the 28th of December 2021 and received the registration code BC-11330. Patients were asked to give oral and written informed consent for skin sample collection.

Author contributions

Anna Szabó was responsible for conceptualization, the development of the MN arrays with regard to material selection, development and characterization, MN fabrication and characterization, along with Sam Samey, and preparation of the manuscript.

Ignace De Decker was responsible for conceptualization, the *ex vivo* evaluation of the developed MN arrays, along with Sam Samey, and preparation of the manuscript.

Karel E.Y. Claes, Phillip Blondeel, Stan Monstrey, Jo Van Dorpe and Sandra Van Vlierberghe were responsible for conceptualization, along with evaluating the experimental plan, development of the MN arrays and contributed to the preparation of the manuscript.

Supporting Information

Supporting Information is available from the Online Library or from the authors.

Funding

This research has received funding from the European Union's Horizon 2020 research and innovation program under grant agreement No 828835.

Data availability statement

The data gained during the preparation of the manuscript are available upon request from the corresponding author, Sandra Van Vlierberghe.

References

Andersen TE, Andersen AJ, Petersen RS, et al. (2018). Drug loaded biodegradable polymer microneedles fabricated by hot embossing. Microelectron Eng 195:1–17. doi:10.1016/j.mee.2018.03.024.

Lorden ER, Miller KJ, Bashirov L, et al. (2015). Mitigation of hypertrophic scar contraction via an elastomeric biodegradable scaffold. Biomaterials 43:61–70. doi:10.1016/j.biomaterials.2014.12.003.

Johnson PM, Meinhold KL, Ohl NR, et al. (2022). Surfactant molecular properties control location in emulsion electrospun fibers and dictate resulting fiber properties. Macromolecules 55:9186–95. doi:10.1021/acs.macromol.2c00998.

Aldawood FK, Andar A, Desai S. (2021). A comprehensive review of microneedles: Types, materials, processes, characterizations and applications. Polymers (Basel) 13:2815. doi:10.3390/polym13162815.

Arslan A, Steiger W, Roose P, et al. (2021). Polymer architecture as key to unprecedented high-resolution 3D-printing performance: The case of biodegradable hexa-functional telechelic urethane-based poly-ε-caprolactone. Mater Today 44:25–39. doi:10.1016/j.mattod.2020.10.005.

Bhadale RS, Londhe VY. (2021). A systematic review of carbohydrate-based microneedles: current status and future prospects. J Mater Sci Mater Med 32:89–106. doi:10.1007/s10856-021-06559-x.

Buthylated hydroxytoluene, Safety data sheet - Buthylated hydroxytoluene. (n.d). Safety data sheet. https://www.sigmaaldrich.com/BE/en/sds/aldrich/w218405.

Cheng J, Chen G, Zhu Y. (2017). Fe3O4/polycaprolactone microneedles with controlled drug delivery and magnetic hyperthermia. Nano Adv 2:29–35. doi:10.22180/na200.

Claeys B, Vervaeck A, Hillewaere XKD, et al. (2015). Thermoplastic polyurethanes for the manufacturing of highly dosed oral sustained release matrices via hot melt extrusion and injection molding. Eur J Pharm Biopharm 90:44–52. doi:10.1016/j.ejpb.2014.11.003.

Costa ED, Priotti J, Orlandi S, et al. (2016). Unexpected solvent impact in the crystallinity of praziquantel/poly(vinylpyrrolidone) formulations. A solubility, DSC and solid-state NMR study. Int J Pharm 511:983–93. doi:10.1016/j.ijpharm.2016.08.009.

De Decker I, Beeckman A, Hoeksema H, et al. (2023a). Pressure therapy for scars: Myth or reality? A systematic review. Burns 49:741–56. doi:10.1016/j.burns.2023.03.007.

De Decker I, Hoeksema H, Vanlerberghe E, et al. (2023b). Occlusion and hydration of scars: moisturizers versus silicone gels. Burns 49:365–79. doi:10.1016/j.burns.2022.04.025.

De Decker I, Logé T, Hoeksema H, et al. (2023c). Dissolving microneedles for effective and painless intradermal drug delivery in various skin conditions: A systematic review. J Dermatol 50:422–44. doi:10.1111/1346-8138.16732.

De Decker I, Szabó A, Hoeksema H, et al. (2023d). Treatment of Hypertrophic Scars with Corticoid-Embedded Dissolving Microneedles. J Burn Care Res 44:158–69. doi:10.1093/jbcr/irac165.

Du G, Sun X. (2020). Current advances in sustained release microneedles. Pharm Fronts 02:e11–e22. doi:10.1055/s-0040-1701435.

Gainanova GA, Zhil'tsova EP, Kudryavtseva LA, et al. (2006). Aggregation and catalysis in a nonionic surfactant-polyethylenimine-chloroform system. Colloid J 68:533–40. doi:10.1134/S1061933X06050024.

Gauglitz GG, Korting HC, Pavicic T, et al. (2011). Hypertrophic scarring and keloids: pathomechanisms and current and emerging treatment strategies. Mol Med 17:113–25. doi:10.2119/molmed.2009.00153.

Hardy IJ, Cook WG, Melia CD. (2006). Compression and compaction properties of plasticised high molecular weight hydroxypropylmethylcellulose (HPMC) as a hydrophilic matrix carrier. Int J Pharm 311:26–32. doi:10.1016/j.ijpharm.2005.12.025.

Heng WSP, Wan LSC, Ang TSH. (1990). Role of surfactant on drug release from tablets. Drug Dev Ind Pharm 16:951–62, doi: 10.3109/03639049009114921.

Houben A, Van Vlierberghe S, Dubruel P. (2014). *Novel urethane based materials, derivatives, methods of their preparation and uses*. International Application PCT/EP2016/065391, 30 June.

Izumikawa S, Yoshioka S, Aso Y, Takeda Y. (n.d). Preparation of poly (l-lactide) microspheres of different crystalline morphology and effect of crystalline morphology on drug release rate. J Control Release15:133–40

Jiang Z, Zhao L, He F, et al. (2021). Palmatine-loaded electrospun poly(ε-caprolactone)/gelatin nanofibrous scaffolds accelerate wound healing and inhibit hypertrophic scar formation in a rabbit ear model. J Biomater Appl 35:869–86. doi:10.1177/0885328220950060.

Kapourani A, Tzakri T, Valkanioti V, et al. (2021). Drug crystal growth in ternary amorphous solid dispersions: Effect of surfactants and polymeric matrix-carriers. Int J Pharm X 3:100086. doi:10.1016/j.ijpx.2021.100086.

Khan S, York P, Shah M, Khan J. A Stable Hydrocortisone Nanosuspension for Improved Dissolution: Preparation, Characterization and In Vitro Evaluation Vitiligo and Melasma View project Natural herbal medicines View project, (2017). https://www.researchgate.net/publication/319528720.

Ko P-T, Lee I-C, Chen M-C, Tsai S-W. (n.d). Polymer microneedles fabricated from PCL and PCL/PEG blends for transdermal delivery of hydrophilic compounds. J Taiwan Inst Chem Eng 51:1–8. doi:10.1016/j.jtice.2015.01.003.

Koyani RD. (2020). Synthetic polymers for microneedle synthesis: from then to now. J Drug Deliv Sci Technol 60:102071. doi:10.1016/j.jddst.2020.102071.

Lin S, Quan G, Hou A, et al. (2019). Strategy for hypertrophic scar therapy: improved delivery of triamcinolone acetonide using mechanically robust tip-concentrated dissolving microneedle array. J Control Release 306:69–82. doi:10.1016/j.jconrel.2019.05.038.

Li X, Xu Q, Zhang P, et al. (2019). Cutaneous microenvironment responsive microneedle patch for rapid gene release to treat subdermal tumor. J Control Release 314:72–80. doi:10.1016/j.jconrel.2019.10.016.

Mondal D, Griffith M, Venkatraman SS. (2016). Polycaprolactone-based biomaterials for tissue engineering and drug delivery: current scenario and challenges. Int J Polym Mater Polym Biomater 65:255–65. doi:10.1080/00914037.2015.1103241.

Nagarkar R, Singh M, Nguyen HX, Jonnalagadda S. (2020). A review of recent advances in microneedle technology for transdermal drug delivery. J Drug Deliv Sci Technol 59:101923. doi:10.1016/j.jddst.2020.101923.

O'Neil, MJ. (2021). The Merck Index: An encyclopedia of chemicals, drugs, and biologicals. 13th ed. NJ, Merck: Whitehouse Station.

Orozco-Castellanos LM, Marcos-Fernández A, Martínez-Richa A. (2011). Hydrolytic degradation of poly(ε-caprolactone) with different end groups and poly(ε-caprolactone-co-γ-butyrolactone): Characterization and kinetics of hydrocortisone delivery. Polymers for Advanced Techs 22:430–6. doi:10.1002/pat.1531.

Park J-H, Allen MG, Prausnitz M. (2005). Biodegradable polymer microneedles fabrication mechanics and transdermal drug delivery. J Control Release 104:51–66. doi:10.1016/j.jconrel.2005.02.002.

Park JH, Allen MG, Prausnitz MR. (2006). Polymer microneedles for controlled-release drug delivery. Pharm Res 23:1008–19. doi:10.1007/s11095-006-0028-9.

Phenotiazine, Safety data sheet - Phenotiazine, Safety Data Sheet. (n.d). https://www.sigmaaldrich.com/BE/en/sds/aldrich/p14831 (accessed May 18, 2023).

Prausnitz MR. (2004). Microneedles for transdermal drug delivery. Adv Drug Deliv Rev 56:581–7. doi:10.1016/j.addr.2003.10.023.

Qi S, Roser S, Edler KJ, et al. (2013). Insights into the role of polymer-surfactant complexes in drug solubilisation/stabilisation during drug release from solid dispersions. Pharm Res 30:290–302. doi:10.1007/s11095-012-0873-7.

Rask MB, Knopp MM, Olesen NE, et al. (2018). Comparison of two DSC-based methods to predict drug-polymer solubility. Int J Pharm 540:98–105. doi:10.1016/j.ijpharm.2018.02.002.

Solaiman DKY, Ashby RD, Zerkowski JA, et al. (2015). Control-release of antimicrobial sophorolipid employing different biopolymer matrices. Biocatal Agric Biotechnol 4:342–8. doi:10.1016/j.bcab.2015.06.006.

Tan CWX, Tan WD, Yow RSAP, Wong DWK, Tey HL. (n.d). Dissolving triamcinolone-embedded microneedles for the treatment of keloids: a single-blinded intra-individual controlled clinical trial. doi:10.6084/m9.figshare.9009647.

Thijssen Q, Parmentier L, Augustyniak E, et al. (2022). From chain growth to step growth polymerization of photoreactive poly-ε-caprolactone: the network topology of bioresorbable networks as tool in tissue engineering. Adv Funct Mater 32:1–14. doi:10.1002/adfm.202108869.

Triphenylphosphine. (n.d). Safety Data Sheet - EN - (23253991) TRIPHENYLPHOSPHINE. (TPP) [603-35-0], Safety Data Sheet.

Van Renterghem J, Dhondt H, Verstraete G, et al. (2018). The impact of the injection mold temperature upon polymer crystallization and resulting drug release from immediate and sustained release tablets. Int J Pharm 541:108–16. doi:10.1016/j.ijpharm.2018.01.053.

Vermoesen E, Cordeels E, Schaubroeck D, et al. (2023). Photo-crosslinkable biodegradable polymer coating to control fertilizer release. Eur Polym J 186:111835. doi:10.1016/j.eurpolymj.2023.111835.

Wang L, Yang J, Ran B, et al. (2017). Small molecular TGF-β1-inhibitor-loaded electrospun fibrous scaffolds for preventing hypertrophic scars. ACS Appl Mater Interf 9:32545–53. doi:10.1021/acsami.7b09796.

Wei-Ze L, Mei-Rong H, Jian-Ping Z, et al. (2010). Super-short solid silicon microneedles for transdermal drug delivery applications. Int J Pharm 389:122–9. doi:10.1016/j.ijpharm.2010.01.024.

Yavuz B, Chambre L, Harrington K, et al. (2020). Silk fibroin microneedle patches for the sustained release of levonorgestrel. ACS Appl Bio Mater 3:5375–82. doi:10.1021/acsabm.0c00671.